

Normal and lateral modulation with a scanning force microscope, an analysis: implication in quantitative elastic and friction imaging

Pierre-Emmanuel Mazeran and Jean-Luc Loubet

Laboratoire de Tribologie et Dynamique des Systèmes – UMR CNRS 5513, Ecole Centrale de Lyon, BP 163, 69131 Ecully Cedex, France
E-mail: mazeran@ec-lyon.fr

Received 2 November 1997; accepted 8 November 1999

Results and an analysis are presented on elastic and friction imaging by indirect force modulation with a scanning force microscope. Two techniques are compared, normal modulation (Z -modulation, perpendicular to the surface of the sample) and lateral modulation of the contact (X -modulation in the plane of the sample, perpendicular to the axis of the cantilever). Theoretical and experimental results show that lateral modulation offers great advantages compared to normal modulation: the images are free of artifacts and can be easily quantified.

Keywords: scanning force microscope, lateral force microscope, force modulation, normal and lateral modulation, elasticity, friction, contact stiffness, Young modulus, shear modulus, modeling

1. Introduction

Since its invention in 1986 [1], the scanning force microscope (SFM), also called atomic force microscope (AFM), has been developed to produce image maps of mechanical properties at the nanometer scale. The most notable extension of contact SFM is probably the development of the lateral force microscope (LFM), which is able to measure quantitatively the friction force between the tip and the sample [2–8], and the development of the force modulation microscope (FMM) technique which opened the field of qualitative analysis of the elasto-plastic properties of the sample [9–15].

The principle of FMM is to create a harmonic modulation force on the contact, of some amplitude on top of the static applied force, and to measure the harmonic response of the cantilever. Two types of FMM, indirect [9–12] or direct [13–15] mode, can be used. In the case of direct FMM, the force acts directly on the cantilever whereas for indirect FMM, the modulation is achieved via a vertical modulation of the sample (or cantilever) position. In indirect FMM, the modulation could be normal (Z -modulation) or lateral (X -modulation) to the sample (figure 1), but only Z -modulation is commercially available and currently used. Nevertheless, some limitations of the Z -modulation technique can be noticed:

- (1) The major default of the Z -modulation technique is due to the laser beam detection system. The Z -modulation induces a tilt of the cantilever and then a Y -modulation of the tip. The Y -movement of the tip leads to a lateral force. Because the “A-B” signal is sensitive to the change of angle at the edge of the cantilever, the “A-B” signal is sensitive to the normal and lateral force applied on the tip. It is why lateral stiffness and/or fric-

tion forces could influence FMM experiments [15,16]. So in the simplest case, three regimes can be obtained depending on the Z -modulation operating conditions: first an elastic indentation regime, second a lateral elastic regime and third a lateral friction regime. These three regimes are not well separated and the response of the cantilever is a complex combination of them. The influence of the operating conditions (amplitude, angles between the lever and the surface, geometrical and mechanical properties of the lever and the mechanical properties of the material) on these three regimes are not well known. So, due to the lack of a model that takes into account the lateral force, no relation could be given between the response of the cantilever and the elasticity of the surface. These limitations lead to much difficulty to realize quantitative imaging and sometimes true elastic imaging. As an example strong friction influence has been discussed [16].

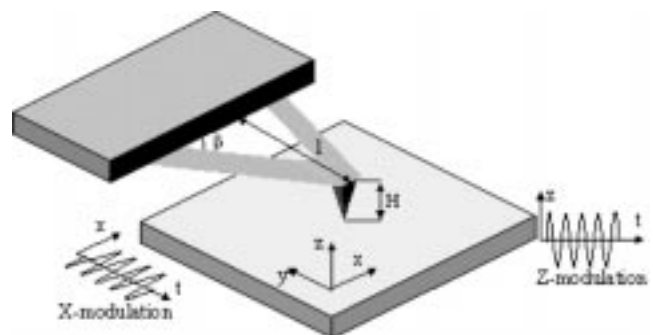


Figure 1. Schematic of FMM. The sample is modulated in the z or x axis. The response of the cantilever depends on normal or lateral contact stiffness (if the excitation is small enough) for Z -modulation and X -modulation, respectively.

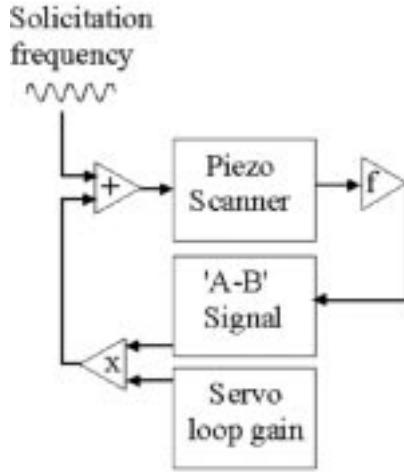


Figure 2. In Z -modulation, the cantilever response is amplified by the servo-loop and re-injected in the scanner so added to the original excitation. The consequence is that the cantilever is solicited by a complex input and leads to poor quality imaging.

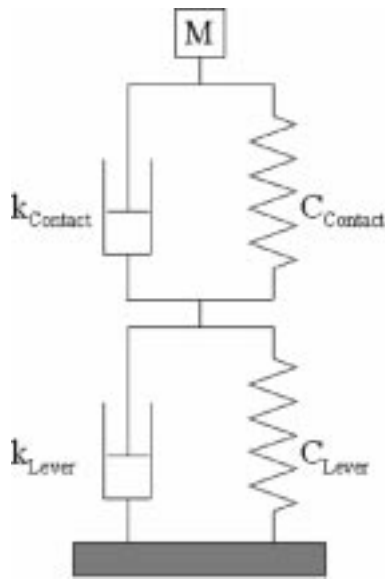


Figure 3. Schematic of the “two Kelvin–Voigt” mechanical equivalent model. The two Kelvin–Voigt elements (built with a spring of stiffness k and a damper of damping constant C correspond to the mechanical properties of the cantilever and of the contact.

(2) The excitation of the contact leads to a response of the cantilever and then, to the appearance of a harmonic signal on the “A–B” signal. Because the “A–B” is the input of the servo loop, the piezo is also excited by this signal which creates a sub excitation of the piezo (figure 2). This phenomenon leads to poor quality imaging due to noise. This is why higher quality FMM imaging is obtained with a two-piezo system at high frequency. In this system, two piezos are used; the first one is used to monitor the position of the sample whereas the other one is only used for the excitation of the contact. The frequency is chosen to give a good response on the extra piezo and a low response on the monitor position piezo.

Nomenclature

a :	contact radius
A :	ratio of the lateral contact stiffness on the normal contact stiffness
d :	lateral movement
d^* :	amplitude of a harmonic lateral movement
C :	LFM calibration parameter
D :	limit displacement between partial slip and total slip
ΔS :	Z -movement of the sample
ΔY :	Y -movement of the tip
ΔZ :	Z -movement of the lever
$\Delta\Theta$:	angle change of the lever
e :	meniscus radius
E :	Young modulus
E^* :	reduced Young modulus
f :	first flexion resonance frequency of the cantilever
F_{Cap} :	capillary force
F_F :	friction force
F_L :	lateral force
F_N :	normal force
g :	liquid film thickness
G :	shear modulus
G^* :	reduced shear modulus
H :	tip height
I :	moment of inertia
k_B :	buckling cantilever stiffness
k_F :	flexion cantilever stiffness
k_L :	lateral contact stiffness
k_L^* :	lateral system stiffness
k_N :	normal contact stiffness
k_N^* :	normal system stiffness
k_T :	torsion cantilever stiffness
L :	length of the cantilever
n :	ratio of the normal contact stiffness to the flexion cantilever stiffness
M :	applied couple
M^* :	equivalent mass of the cantilever
N :	normal force
P_m :	average pressure
R :	radius
R^* :	equivalent radius
α :	angle between the cantilever and the sample in the Y -direction
β :	angle between the cantilever and its substrate
δ :	elastic deformation
ξ_0 :	atomic equilibrium distance
γ :	angle between the cantilever and the sample in the X -direction
γ_{LV} :	surface tension of a liquid
λ :	Maugis parameter
ν :	Poisson ratio
w :	work of adhesion

(3) The equivalent model proposed for indirect FMM, is a series arrangement of two Kelvin–Voigt elements [13,17] (figure 3). The system compliance is equal to the sum of the compliance of the two springs modeling both contact stiffness and cantilever stiffness. For Z -modulation experiments:

$$k_N^* = \left(\frac{1}{k_N} + \frac{1}{k_F} \right)^{-1}, \quad (1)$$

with k_N the normal contact stiffness and k_F the cantilever stiffness.

According to the “two Kelvin–Voigt” model the vertical movement of the tip ΔZ , for quasi-static measurement with

a low modulation and without damping [9] should be equal to

$$\Delta Z = \frac{n}{n+1} \Delta S, \quad (2)$$

with ΔS the Z -modulation of the sample, and n the ratio of the normal contact stiffness k_N to the cantilever flexion stiffness k_F :

$$n = \frac{k_N}{k_F}. \quad (3)$$

As a consequence, for a good sensitivity the cantilever stiffness must be at least of the same order of magnitude of the normal contact stiffness which is typically about 10–1000 N m⁻¹. For example, according to the DMT theory (see section 3), if the equivalent radius R^* is equal to 50 nm, the normal force equal to 1 nN, and the equivalent elastic modulus E^* equal to 3 GPa, the normal contact stiffness k_N is close to 14 N/m.

Recently Rabe et al. [18] have shown the limitation of the “two Kelvin–Voigt” model and proposed a model which integrates the mechanical properties of the lever. Still more recently, Mazeran and Loubet [15] have proposed a similar model that also integrates the tangential properties of the contact.

In this paper, we discuss some artifacts and introduce a model that takes into account the lateral contact stiffness and the friction force. This model, as well as experimental results, shows that it is difficult to obtain true and quantitative elastic imaging using Z -modulation. In order to improve this limitation, we proposed the X -modulation technique that gives true and quantitative elastic imaging.

2. Contact theories

We consider two elastic spheres in contact, of radius R_1 and R_2 , made of isotropic materials of Young modulus E_1 and E_2 , and Poisson ratio ν_1 and ν_2 . We define R^* as the reduced radius, E^* as the reduced Young modulus and G^* as the reduced shear modulus:

$$R^* = \left(\frac{1}{R_1} + \frac{1}{R_2} \right)^{-1}, \quad (4)$$

$$E^* = \left(\frac{1-\nu_1^2}{E_1} + \frac{1-\nu_2^2}{E_2} \right)^{-1} \quad (5)$$

and

$$G^* = \left(\frac{2-\nu_1}{G_1} + \frac{2-\nu_2}{G_2} \right)^{-1} \quad (6)$$

with

$$G = \frac{E}{2(1+\nu)}. \quad (7)$$

In the case of an elastic contact where surface forces act, two theories should be considered if the load is comparable to the adhesive force. In the Johnson, Kendall and

Roberts (JKR) theory [19], adhesion forces outside the contact are neglected whereas for the Derjaguin, Muller and Toporov (DMT) theory [20] the adhesion force acts outside the contact area and is not able to deform the surface. Recently, Maugis proposed a continuous transition between the JKR theory and the DMT theory using the Dugdale approximation [21]. Maugis proposed a non-dimensional parameter λ to establish the domains of validity of the JKR–DMT theories. This parameter compares the elastic deformation δ due to adhesive force to the atomic equilibrium distance ξ_0 :

$$\lambda = \frac{8}{3\sqrt{3}} \sqrt[3]{\frac{4}{3} \frac{R^* w^2}{\pi E^* \xi_0^3}} \approx \frac{3}{2} \frac{\delta}{\xi_0}, \quad (8)$$

with w the work of adhesion.

Maugis shows that the JKR theory is valid if λ is greater than 3 and the DMT theory should be applied if λ is less than 0.1.

During a SFM experiment in air, a capillary force F_{Cap} is added to the surface force:

$$F_{\text{Cap}} = 4\pi R^* \gamma_{\text{LV}}, \quad (9)$$

with γ_{LV} the surface tension.

As done by Maugis for the DMT–JKR transition, we proposed to compare the elastic deformation due to the meniscus pressure to the equilibrium atomic distance. The average pressure p_m due to the meniscus is equal to

$$p_m = \frac{F_{\text{Cap}}}{\pi e^2} = \frac{4R^* \gamma_{\text{LV}}}{e^2}, \quad (10)$$

where e is the radius of the meniscus. This depression leads to an elastic deformation δ of the two surfaces [22]:

$$\delta = \frac{4p_m e}{\pi E^*} = \frac{16R^* \gamma_{\text{LV}}}{\pi e E^*}. \quad (11)$$

If the thickness of the liquid film on the surface is equal to g on the two surfaces ($g \ll R^*$) we are able to find the radius of the meniscus using the Chord theorem:

$$e = 2\sqrt{R^* g}. \quad (12)$$

The equation becomes

$$\delta = \frac{8\gamma_{\text{LV}}}{\pi E^*} \sqrt{\frac{R^*}{g}} \quad (13)$$

and the DMT/JKR transition criterion becomes

$$\lambda \approx \frac{12\gamma_{\text{LV}}}{\pi \xi_0 E^*} \sqrt{\frac{R^*}{g}}. \quad (14)$$

We consider a silicon nitride tip ($E = 140$ GPa [23] and ξ_0 equal to 0.23 nm), a reduced elastic modulus between 3 and 100 GPa, a tip radius equal to 50 nm, the surface tension of water (0.072 N/m), and a water film thickness estimated to 1 nm. For high Young modulus ($E^* = 100$ GPa), λ is equal to 0.08 and the DMT theory is valid. For low elastic modulus ($E^* = 3$ GPa), λ is close to 2.7, we are in

the Maugis transition. Nevertheless, to simplify the problem we propose to consider that the DMT theory is always valid.

In this case of the DMT theory, the normal contact stiffness k_N and the lateral contact stiffness k_L are equal to

$$k_N = 2E^*a, \quad (15)$$

$$k_L = 8G^*a, \quad (16)$$

where a is the radius of contact:

$$a = \sqrt[3]{\frac{3}{4} \frac{R^*(F_N + F_{\text{Cap}})}{E^*}}. \quad (17)$$

For isotropic homogeneous materials, the Poisson ratio varies from 0.1 to 0.5¹ [24]. So the ratio of the lateral stiffness to the normal stiffness varies from 2/3 to 18/19 with a typical value of 4/5,

$$\frac{2}{3} \leq \frac{k_L}{k_N} \leq \frac{18}{19}.$$

3. X-modulation

The technique is similar to Z-modulation but imposes only a lateral excitation of the contact. This technique has been first proposed by Maivald et al. [9]. Later, this technique has been developed for friction imaging (high amplitude) [8,25,26] and for elastic measurement (low amplitude) [27–31]. The piezo is modulated in the plane, perpendicularly to the axis of the cantilever. The torsion of the beam is measured via the LFM signal. Because there is no rejection of the LFM signal on the servo loop (if we assume that the LFM signal is only sensitive to the torsion of the cantilever), this technique does not need an other piezo and could be used at lower frequency as compared to Z-modulation.

The “two Kelvin–Voigt” model could be applied for X-modulation experiments; in this case the system lateral stiffness is equal to

$$k_L^* = \left(\frac{1}{k_L} + \frac{1}{k_T} \right)^{-1}, \quad (18)$$

where k_T is the cantilever torsion stiffness and k_L the lateral contact stiffness. The advantages of lateral modulation have been discussed by Carpick et al. [28]. The major one is to replace, in the “two Kelvin–Voigt” model, the flexion stiffness by the torsion stiffness which is well higher than the flexion stiffness (see below) whereas the lateral and normal contact stiffness are of the same order of magnitude (see section 2).

The relation between the torsion cantilever stiffness k_T and the flexion cantilever stiffness k_F for a rectangular beam is given by the following formula:

$$\frac{k_T}{k_F} = \frac{2}{3(1+\nu)} \left(\frac{L}{H} \right)^2 \approx 0.5 \left(\frac{L}{H} \right)^2, \quad (19)$$

¹ For composite or biological materials, the Poisson ratio could be negative. See, for example, [24].

where ν the Poisson ratio ($\nu = 0.27$ [32] for silicon nitride cantilever), L the length of the cantilever and H the height of the tip. Recently Noy et al. [33] have proposed an equation that gives the relation between the flexion and the torsion stiffness for triangular shape cantilever:

$$\frac{k_T}{k_F} = \frac{2}{6 \sin^2(\beta) + 3(1+\nu) \cos^2(\beta)} \left(\frac{L}{H} \right)^2 \approx 0.35 \left(\frac{L}{H} \right)^2, \quad (20)$$

with β the angle between the cantilever and its substrate (typically 65°) (figure 1). This formula has been validated experimentally by Ogletree et al. [32].

The ratio of the length of the cantilever to the tip height is typically between these two limits:

$$100 \leq \frac{L}{H} \leq 20.$$

Then the torsion stiffness is generally two or three orders of magnitude higher than the flexion stiffness. Typically $k_T/k_F = 100$ for high cantilever flexion stiffness, and 4000 for low cantilever flexion stiffness (see table 1 for details).

4. Experimental

4.1. Materials and methods

We used a commercial contact SFM (Autoprobe CP, Park Scientific Instruments, USA) with a LFM head and a “signal access module” option. The cantilevers used are silicon or silicon nitride cantilevers (Microlever and Ultra-lever, Park Scientific Instruments, USA) with flexion stiffness from 0.01 to 18 N m⁻¹. The nominal radii of the tips are 20 and 50 nm, respectively (see table 1 for details).

The SFM piezo tube or an extra piezo (PXE5, Philips, The Netherlands) achieves the excitation of the contact. A frequency generator feeds the piezo and a lock-in amplifier analyzes the output signal (“A-B” or LFM signal). All images presented are untreated.

A composite material made of carbon fibers ($E = 40$ GPa) and an epoxy matrix ($E = 3$ GPa) has been used as sample. The two materials are amorphous and supposed to be isotropic. The values of the elastic modulus have been estimated using a nanoindentation experiment. The sample has been polished in order to limit the topographic artifacts.

4.2. Z-modulation imaging

Z-modulation images realized with high cantilever stiffness ($k_F = 13$ N m⁻¹) present the contrast predicted by the “two Kelvin–Voigt” model. The carbon fibers give a higher response (figure 4). Nevertheless, contrast in Z-modulation image is obtained with low cantilever stiffness ($k_F = 0.1$ N m⁻¹), whereas the “two Kelvin–Voigt” model predicts no contrast in FMM images (figure 5):

Table 1

Geometrical and mechanical properties of cantilevers. Microlevers are silicon nitride cantilevers ($E = 140 \pm 10$ GPa) with a pyramidal tip (radius 50 nm, $H = 3 \mu\text{m}$). Ultralevers are silicon cantilevers ($E = 125$ GPa) with a conical tip (radius 20 nm, $H = 4 \mu\text{m}$). Data are reported from the manufacturer sheet, except for angle and torsion stiffness.

Cantilever	Shape	Length (μm)	Width (μm)	Thickness (μm)	Flexion stiffness (N m^{-1})	Angle ($^\circ$)	Torsion stiffness calculated using formula (20) (N m^{-1})
Microlever A	Triangular	180	18	0.6 ± 0.1	0.03–0.08	67	32–82
Microlever B	Rectangular	200	20	0.6 ± 0.1	0.01–0.03		19–54
Microlever C	Triangular	320	22	0.6 ± 0.1	0.006–0.015	71	20–48
Microlever D	Triangular	220	22	0.6 ± 0.1	0.02–0.05	72	31–75
Microlever E	Triangular	140	18	0.6 ± 0.1	0.06–0.15	64	40–94
Microlever F	Triangular	85	18	0.6 ± 0.1	0.3–0.8	65	73–184
Ultralever A	Triangular	180	25	1.8 ± 0.2	1.3–2.6	64	650–1210
Ultralever B	Triangular	180	38	1.8 ± 0.2	2.0–3.8	65	1000–1760
Ultralever C	Triangular	85	18	1.8 ± 0.2	9–18	63	1010–1880
Ultralever D	Triangular	85	28	1.8 ± 0.2	13–25	63	1470–2610
Microlever A*	Triangular	170	36	0.6 ± 0.1	0.06–0.15	64	59–139
Microlever B*	Triangular	85	16	0.6 ± 0.1	0.3–0.8	63	74–186

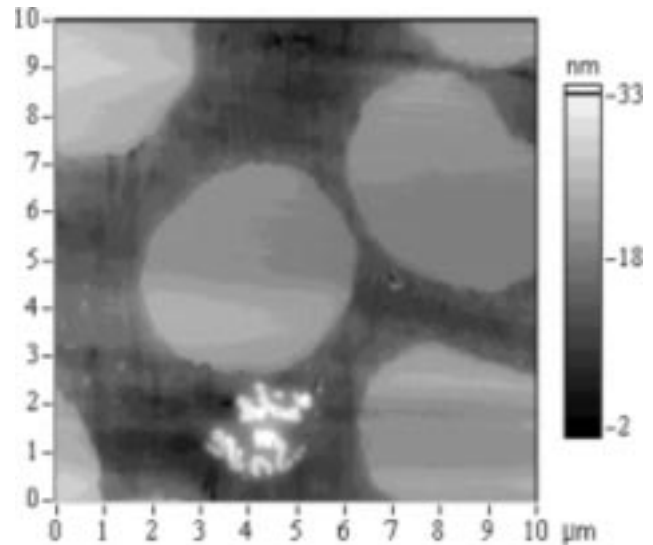
for example, if we apply the DMT model (equations (4), (5), (15) and (17)) we find that the contact stiffness for the epoxy matrix should be equal to about 83 N m^{-1} ($F_N = 0$, $F_{\text{Cap}} = 70 \text{ nN}$, $R = 50 \text{ nm}$, $E^* = 3 \text{ GPa}$) and 296 N m^{-1} ($F_N = 0$, $F_{\text{Cap}} = 30 \text{ nN}$, $R = 50 \text{ nm}$, $E^* = 31 \text{ GPa}$) for the carbon fibers. The difference of the cantilever response (equations (2) and (3)) for the epoxy matrix and for the carbon fibers should be about 0.1% and could not be detected. Furthermore, the contrast is inverted and the image is very close to the friction image (figure 5). In this last case ($k_F = 0.1 \text{ N m}^{-1}$), we deduce that the contrast in this Z -modulation image is only due to friction forces.

4.3. X -modulation imaging

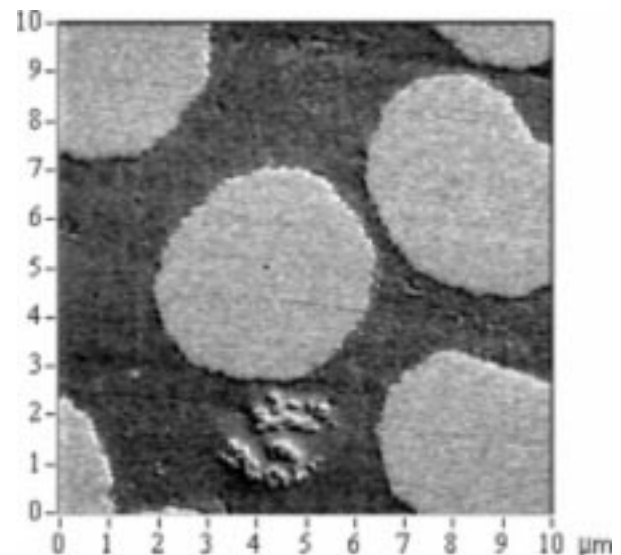
Some limitations occur with the X -modulation technique.

- (i) The image is noisy at frequency lower than 10 kHz, probably due to piezo resonance. Typical values of the frequencies used in this study are 10–40 kHz.
- (ii) The tip velocity generated by X -modulation should be much higher than the velocity generated by the scan. Two solutions are possible: reduce the scan velocity or scan in the Y -direction. We have chosen to scan in the Y -direction.
- (iii) It is important to check if the response is due to elasticity or friction. The best solution is to obtain a friction

Figure 4. Topographic (a) and Z -modulation (b) images on a composite material, carbon fibers (white) in epoxy matrix (black), using high cantilever stiffness ($k_F = 13 \text{ N m}^{-1}$). The jagged island on the bottom of the image is due to a residue of a thin gold layer. The contrast is correct as predicted by the “two Kelvin–Voigt” model: the higher the Young modulus, the higher the response is. The relative response of the cantilever for the two materials is 4–3. Notice the influence of topography on Z -modulation image (10 μm scan, Z -modulation by the monitor piezo, frequency = 10.3 kHz, ultralever type C).



(a)



(b)

image with a high amplitude excitation, to be in a dynamic friction regime, and to measure the response of the cantilever. Then using excitations, which leads to a response ten times lower, we are sure to be in an elastic regime.

In these conditions, we have not observed artifacts using X -modulation or high topographic influence (figure 6). Images obtained with this technique never show inverted contrast (except if the modulation is too high). Furthermore, we are able to observe local changes on the carbon fibers, and also on the epoxy matrix. We believe that these local changes are due to local variations of the elasto-plastic properties of the materials for low modulation and for local changes of the friction properties for high modulation.

4.4. Quantification of the lateral system stiffness

To realize a quantitative experiment three parameters should be known: the stiffness of the cantilever, the radius of the tip and the lateral force.

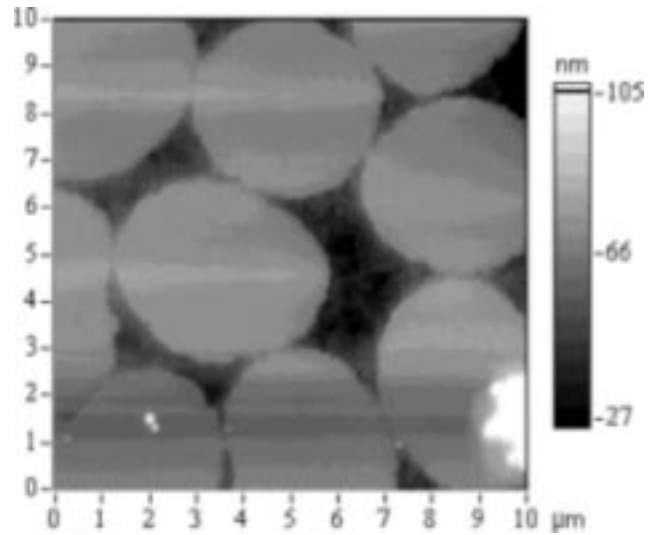
The stiffness of the cantilever is estimated by measuring the first resonance frequency of the cantilever. We assume that only the thickness of the cantilever is not well known [34]. By measuring the first resonance frequency f , we are able to estimate the flexion stiffness of the cantilever:

$$f = \sqrt{\frac{k_F}{M^*}}, \quad (21)$$

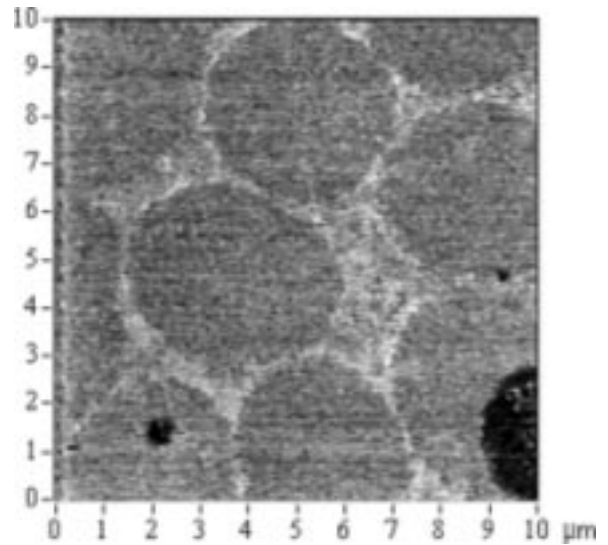
where M^* is the equivalent mass of the cantilever.

The radius of the tip is not directly measured but estimated using a topographic image. During a scan, the tip dilates the features of the surface so that the topographic image is highly influenced by the tip radius. So it is possible to extract the geometry of the tip from a topographic image and to estimate its radius using various techniques [35–37]. We have developed two methods to extract the tip radius from a topographic image [38]. The first method, called maxima method, is based on the principle of erosion. We consider that the features of the SFM image are envelopes of the tip. We used the maxima in height of the feature of the SFM image, which are the only known common points between the image and the surface, as a landmark. Using all the features we obtain an image of the tip, which allows us to eliminate the non-spherical tip and to estimate the tip radius with a precision of a few nanometers. The second method is based on an analysis of the curvature radius of the image. We obtain a radius curvature image from a topographic one and analyze the dominant curvature of this image.

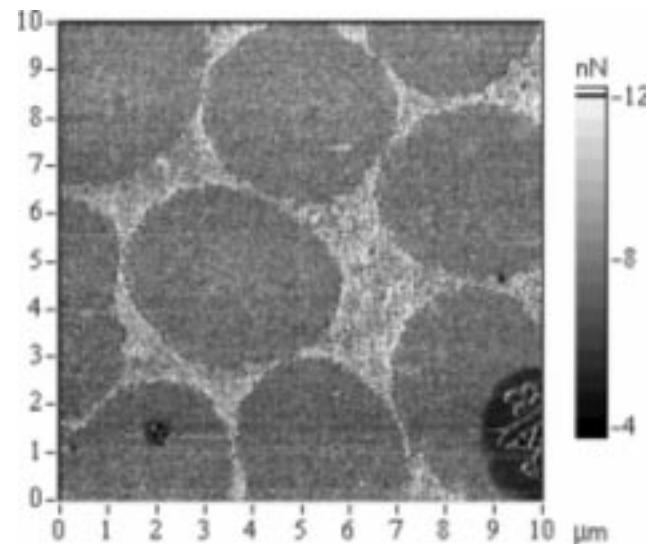
Figure 5. Topographic (a), Z -modulation (b) and LFM (trace minus retrace) (c) on composite material, carbon fibers and epoxy matrix, as imaged by low cantilever flexion stiffness ($k_F = 0.1 \text{ N m}^{-1}$). The contrast of Z -modulation image is inverted in comparison to the contrast predicted by the “two Kelvin–Voigt” model. The correlation between LFM and Z -modulation images makes us think that the same information is contained in the images. ($10 \mu\text{m}$ scan, Z -modulation by the monitor piezo, frequency = 10.3 kHz, microlever type E).



(a)



(b)



(c)

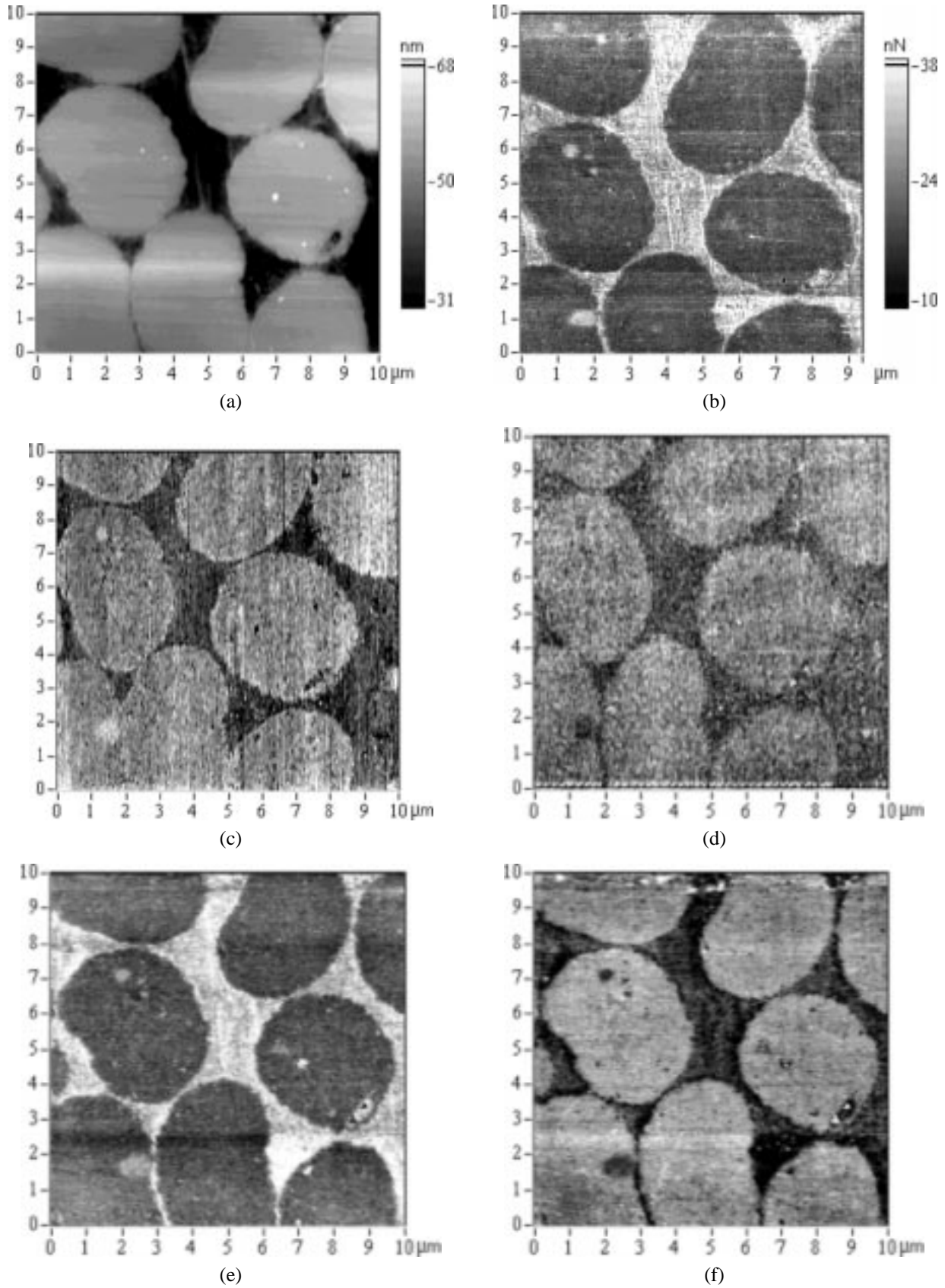


Figure 6. Topographic (a), LFM (trace minus retrace) (b), X-modulation with a low excitation (10 mV) (c), corresponding phase image (d), X-modulation with an higher excitation (100 mV) (e) and corresponding phase image (f) of carbon fibers/epoxy composite. Images (b) and images (e) are friction images whereas image (c) is an elastic image. Note changes of the elastic contrast in image (b) (10 μm scan, X-modulation by the monitor piezo, frequency = 37 kHz, microlever type B*).

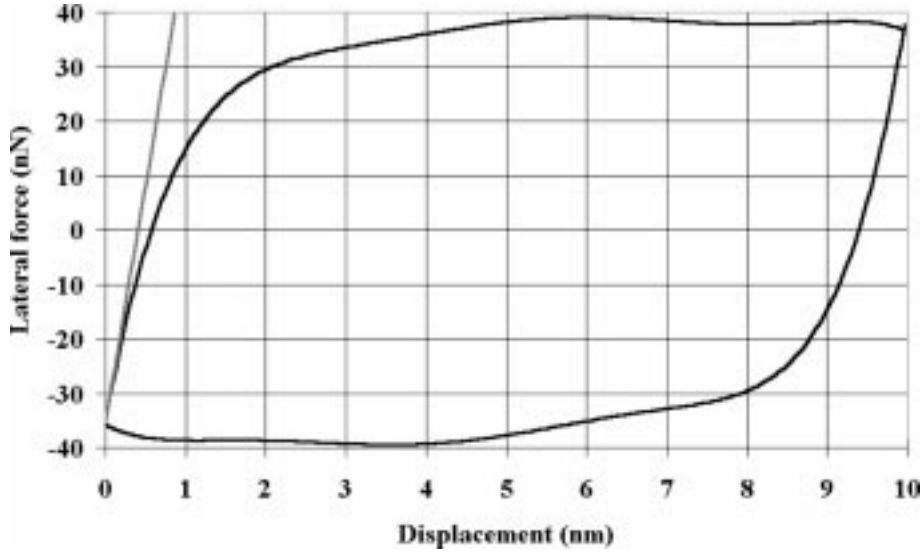


Figure 7. Typical friction loop obtained on the carbon fibers (black line). The slope at the start of the friction loop (gray line), when the tip begins to slip, gives the lateral system stiffness. In this case $k^* = 87 \text{ N m}^{-1}$.

The lateral force is calibrated by measuring the influence of the topography on the lateral force signal [32]. During a scan, the slope of the sample changes so that a component of the normal force F_N is imposed on the lateral force F_L :

$$F_L \approx F_N \tan \gamma + F_F, \quad (22)$$

with F_F the friction force and γ the angle between the sample surface and the cantilever in the direction X . This equation is only valid if $\tan \gamma^* F_F / F_N$ is small compared to one. So the contrast in LFM images contains both information from friction force and from the slope of the surface. Furthermore, the LFM signal is a direct function of the lateral force applied to the tip:

$$\text{LFM} = C(F_N \tan \gamma + F_F), \quad (23)$$

with C the parameter to be calibrate. Assuming the friction force to be constant and the normal force known, the comparison between the topographic image derived in the X -direction and the LFM image gives the value of C and the ability to calibrate the LFM signal.

An X -modulation image with a low excitation could be quantified in terms of lateral system stiffness and Young modulus. Using a friction loop (figure 7) and the Mindlin theory [39] (there is no clue that the Mindlin theory is valid and we do not want to discuss about which theory should be applied since this would exceed the scope of this paper), we are able to estimate the system stiffness: The ratio of the variation of the lateral force to the variation of the lateral displacement, when the tip begins to slip, gives the lateral system stiffness. We measure a system stiffness of 87 and 59 N m^{-1} for the carbon fibers and the matrix, respectively, for a cantilever deflection equal to zero. The total force is then equal to the capillary force.

The flexion cantilever stiffness was estimated to be about 0.5 N m^{-1} and we assume that the cantilever torsion stiffness was about 130 N m^{-1} . Then we find a lateral

Table 2
Estimation of the properties of the contact and of the material, using the X -modulation experiments.

Material	Carbon fibers	Cyano matrix
Lateral system stiffness (N m^{-1})	~ 87	~ 59
Lateral contact stiffness (N m^{-1})	~ 263	~ 108
Capillary force (nN)	~ 30	~ 70
Equivalent Young modulus (GPa)	~ 30	~ 5
Estimated Young modulus (GPa)	~ 38	~ 5
Young modulus (nanoindentation) (GPa)	40	3
Contact radius (nm)	~ 4	~ 11

contact stiffness of 263 and 108 N m^{-1} (equation (17)) for the carbon fibers and the matrix, respectively. The radius of the tip was measured to be about 45 nm. We find a capillary force of about 30 nN for the carbon fibers and about 70 nN for the epoxy matrix. If we apply the DMT theory for a normal force equal to zero, an equivalent radius equal to the radius of the tip and a Poisson ratio equal to 1/3, we find the following relation between the lateral contact stiffness and the equivalent modulus:

$$k_L = \frac{4}{5} k_N = \frac{8}{5} E^* a \approx \sqrt[3]{3E^* R^* F_{\text{Cap}}}. \quad (24)$$

The equivalent Young modulus was measured to be about 30 and 5 GPa, corresponding to a Young modulus of about 38 and 5 GPa (taking a Young modulus of the tip equal to 140 GPa and equation (5)) for the carbon fibers and the epoxy matrix, respectively.

There is a quite good agreement between the measured values and the values measured by nanoindentation experiments (see table 2 for details). The difference between real and measured values could be explained by all the approximations used for the calculations, especially the cantilever stiffness, and by the fact that we are measuring the extreme surface elastic modulus at a nanometer scale.

5. Discussion

5.1. Z-modulation

In order to explain the inverted contrast on the Z-modulation image, we proposed a model that integrates the influence of the lateral force in the Y-axis. This model shows that it is difficult to have a true and quantitative elastic imaging using Z-modulation imaging. This model is based on a rectangular cantilever linked to two springs that model both the normal contact stiffness and the lateral contact stiffness (figure 8). This model does not include viscoelastic effects unlike the works of Frétiigny et al. and Wahl et al. [29–31]. The lateral spring is linked to a shield meaning that the lateral force could not be higher than the friction force. The angle α between the surface and the lever (in the static position) has been taken into account, nevertheless in this paper, we present the equations of a particular case ($\alpha = 0$) to simplify them. We make two approximations: first, the tip is at the edge of the cantilever and second, the change of angle measured by the “A-B” signal is the change of angle at the edge of the cantilever.

If the movement of the sample ΔS (and then the change of angle at the edge of the lever $\Delta\Theta$ and the lateral displacement of the tip ΔY (figure 8)) is small the lateral force is dominated by the lateral system stiffness. The amplitude of vibration of the cantilever is given by the following formula (see appendix A for details):

$$\Delta\Theta = \frac{-\frac{3}{2L}\left(\frac{n}{n+1}\right)}{1 + 3nA\left(\frac{H}{L}\right)^2\left(1 - \frac{3}{4}\frac{n}{n+1}\right)}\Delta S. \quad (25)$$

If ΔS is high, the lateral movement of the tip ΔY is high enough to be in total slip. The lateral force is equal to the friction force. The relation becomes

$$\Delta\Theta = -\frac{3}{2L}\left(\frac{n}{n+1}\right)\Delta S + 3\frac{H}{L^2k_F}\left(1 - \frac{3}{4}\frac{n}{n+1}\right)F_F. \quad (26)$$

It is important to note that the real value is always between the values given by formulas (25) and (26). Figure 9 shows the response of the cantilever as the function of the relative contact stiffness. The response could be decomposed in two domains: For the first domain ($n < 10$ for $\alpha = 15^\circ$), the response of the lever is dominated by the normal contact stiffness. The mechanical behavior of the cantilever is corresponding to a clamped-free beam. In the second domain ($n > 10$ for $\alpha = 15^\circ$) the lateral force is not negligible in front of the buckling stiffness. The mechanical behavior of the cantilever is corresponding to a clamped-hinged beam. For very low excitation (ΔS inferior to a few nanometers, see appendix 1 for details) the response is close to the gray line (figure 9). For very high excitation, the lateral force becomes negligible and the response reaches to the black line. In the real conditions, the response of the cantilever is close to the gray line because

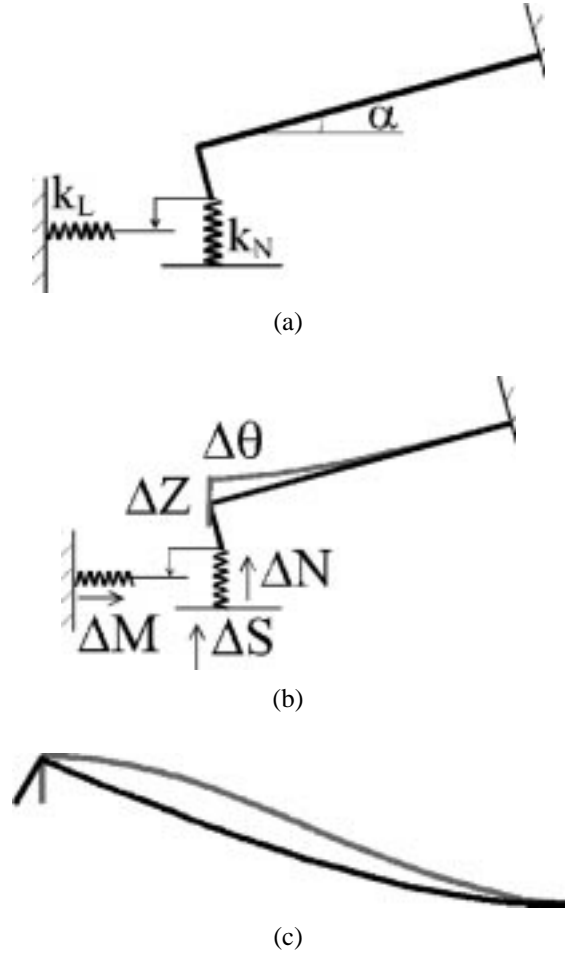


Figure 8. (a) The Z-modulation model is built with a beam linked to two springs that model the normal contact stiffness k_N and the lateral contact stiffness k_L . (b) Forces acting on the cantilever during a Z-modulation. The movement of the piezo leads to a normal force N and then to the flexion of the cantilever. The tilt of the cantilever leads to a movement of the tip and then to a lateral force and an applied couple M . The combination of these two forces is going to change the position ΔZ and the tilt $\Delta\Theta$ of the cantilever. Because, in the laser beam detection system, the “A-B” signal is sensitive to the tilt of the cantilever, the response of the cantilever is sensitive to normal and lateral forces. (c) Shape of a rectangular beam during a Z-modulation experiment. For low $n = k_N/k_F$, the lateral contact stiffness is low compared to the buckling stiffness. The influence of the lateral force is negligible; the shape of the cantilever is corresponding to a clamped-free beam (black line). For high n and small excitation, the lateral contact stiffness is high compared to the buckling stiffness. The tip could not slip freely in the Y-direction. The shape of the cantilever is corresponding to a clamped-guided beam (gray line). In reality the shape of the cantilever is always between the clamped-free and the clamped-guided shape. Then lateral contact stiffness and/or friction force influence the response of the cantilever.

the excitation ΔS is generally small. So the contrast in the image could be due to lateral elasticity and/or friction. As a consequence, the elastic indentation interpretation of the Z-modulation image should be reconsidered for low cantilever stiffness.

From this model we can see that FMM gives an elastic indentation imaging only in the domain where the ratio of the cantilever stiffness to the normal contact stiffness

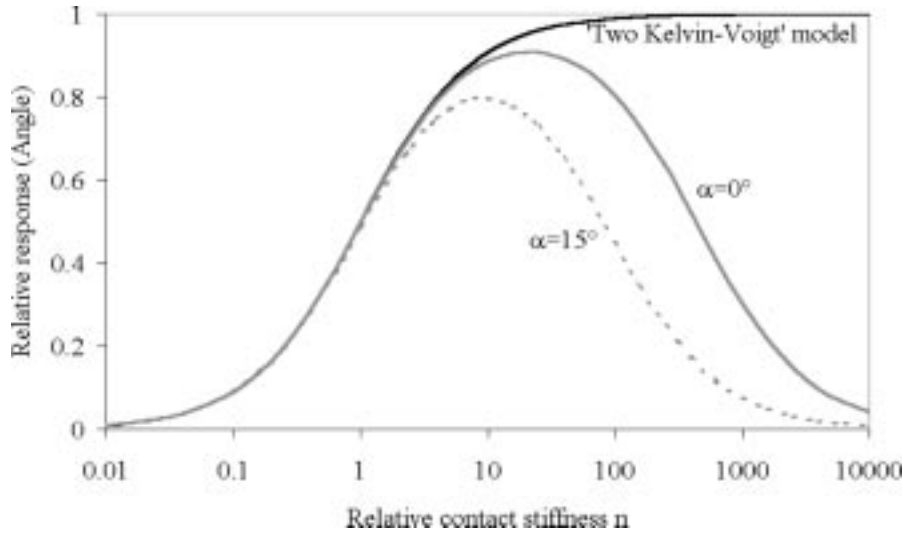


Figure 9. Relative response of the cantilever (change of angle) as a function of the relative contact stiffness $n = k_N/k_F$. The “two Kelvin–Voigt” model (black line) is unable to explain contrast inversion. According to our model, the theoretical response is between the black line and the gray lines. The black line corresponds to infinite modulation; in this case the lateral force becomes negligible. The gray lines correspond to infinite low modulation; in this case the lateral force induced by the lateral contact stiffness is not negligible. The model ($A = k_L/k_N = 0.8$, $H/L = 0.03$, gray solid line for $\alpha = 0^\circ$, gray dashed line for $\alpha = 15^\circ$) shows that the response of the cantilever could be decomposed in two domains: if n is small, the response is only sensitive to indentation elasticity, if n is high, the response is both sensitive to lateral elasticity and to friction.

is inferior to ten. Typically contact stiffness estimated by the DMT theory is between 10 and 1000 N m^{-1} leading to cantilever stiffness of about 10 N m^{-1} value higher than conventional cantilever flexion stiffness. So for classical FMM images, realized with too low cantilever stiffness, we believe that the contrast cannot be attributed to normal contact stiffness but to friction force and/or to the lateral contact stiffness.

Now assume that the Z -movement of the piezo is coupled with a small movement in the Y -direction. A Y -movement of the piezo, in the opposite direction to the direction of sliding induced by the tilt of the cantilever, could change the sign of the lateral force applied on the cantilever. This phenomenon would change the contrast in the Z -modulation image. It is why we believe that the response of the cantilever is highly dependent of the experimental conditions. As the function of them, the amplitude and the sign of the lateral movement changes as well as the response of the cantilever cannot be interpreted.

5.2. X -modulation

During X -modulation the phase signal will not be interpreted as a viscoelasticity effect [29–31] but interpreted as a consequence of the high non-linearity between the lateral force and the lateral displacement. In order to do a good interpretation of the X -modulation signal, we present a theoretical interpretation of the amplitude and phase signal. As an example, we choose the macroscopic Mindlin theory without stick–slip phenomena that seems to be valid experimentally. The same analysis could be realized taking into account other theories [40,41].

When the piezo is modulated in the X -direction, the tip begins to slide only on the periphery of the contact.

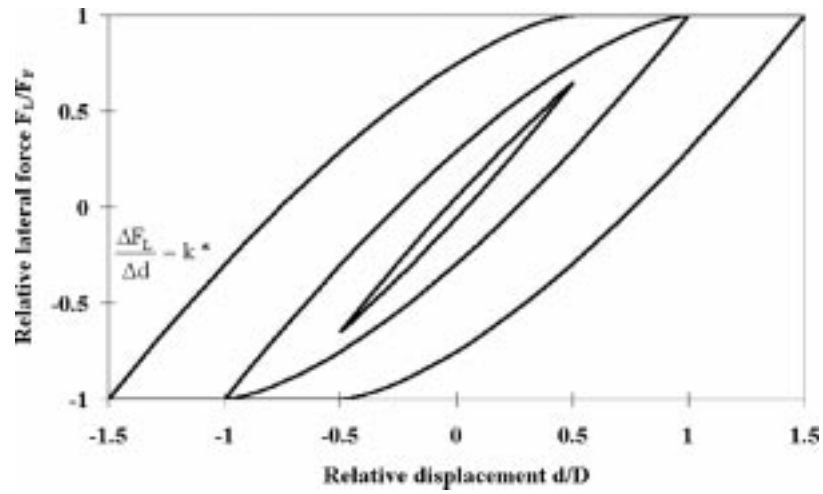
According to the Mindlin theory [42] in the case of an oscillating displacement $d = d^* \cos(\omega t)$, the relation between the lateral force F_L and d becomes

$$\frac{F_L}{F_F} = 2 \left(\frac{2 - d/D - d^*/D}{2} \right)^{3/2} + \left(1 - \frac{d^*}{D} \right)^{3/2} + 1, \quad (27)$$

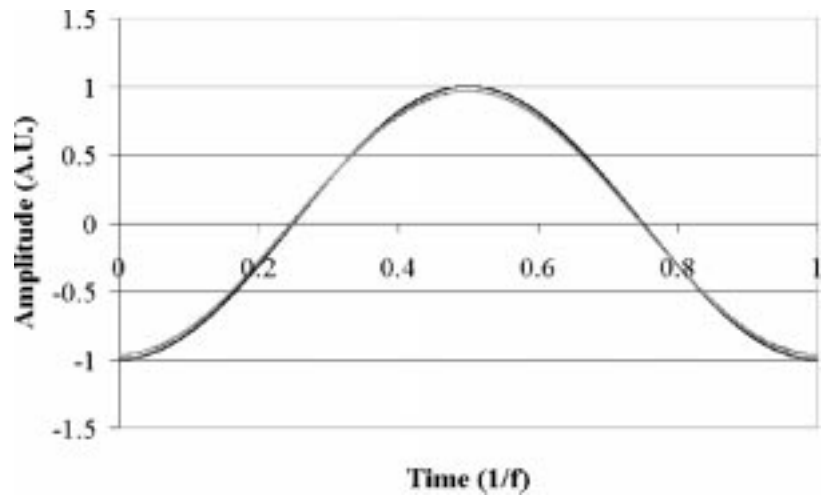
where D is the limit displacement between partial slip and total slip:

$$D = \frac{3}{2} \frac{F_F}{k_L^*}, \quad (28)$$

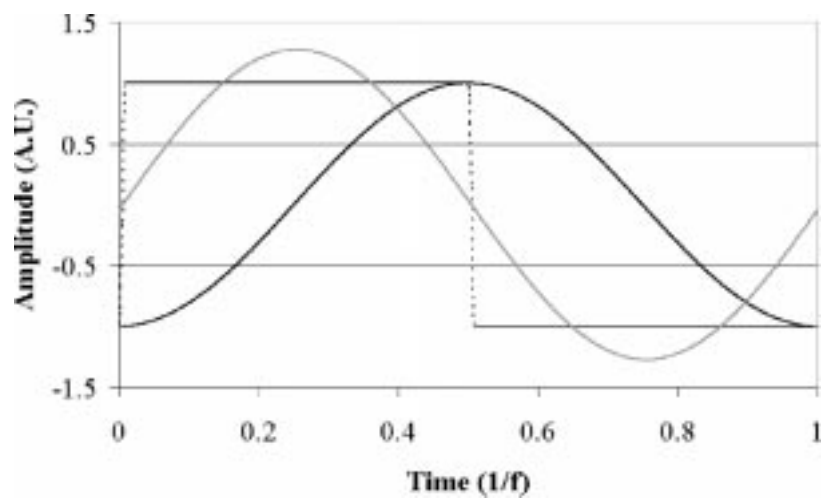
for $d^* < D$ (for $d > D$ then $F_L = F_F$). Figure 10 presents the relation between the lateral force and the displacement for various d^*/D . Then, during an X -modulation experiments, the LFM signal which feeds the lock-in amplifier is no more sinusoidal (figure 10). To interpret the amplitude and the phase images generated during X -modulation experiments, it is important to know how the lock-in amplifier processes a non-sine signal (see appendix B for details). As a result of this processing, the lock-in amplifier gives the amplitude and a phase information that is a function of the first harmonic component of the signal. Colchero et al. has proposed an analysis of the LFM signal in the case of high X -modulation [8]. In the case of low X -modulation, if we consider that there is no viscous effect, the phase information is a direct function of the ratio d^*/D . So the phase image is a direct function of D and then of the ratio of the friction force divided by the lateral system stiffness. Furthermore, for every value of the phase, there is a direct relation between, first, the amplitude (as given by the



(a)



(b)



(c)

Figure 10. Theoretical relative force F_L/F_F as a function of the relative displacement d/D for various displacements d^*/D ($d^*/D = 0.5, 1$ and 1.5 , gray to black curve) according to the Mindlin theory (a). For low excitation ($d^*/D = 0.1$), the tip adheres to the surface, then the displacement and the lateral force are two sine signals in phase (b). For high excitation (c) ($d^*/D = 1000$), the tip slips on the surface, and the lateral force raises abruptly to the friction force. The lateral force becomes a rectangular signal (black dashed line). The lock-in amplifier extracts the first harmonic of this signal (gray line). The relative ratio of the amplitude to the friction force is then equal to $4/\pi$ and the phase is equal to -90° .

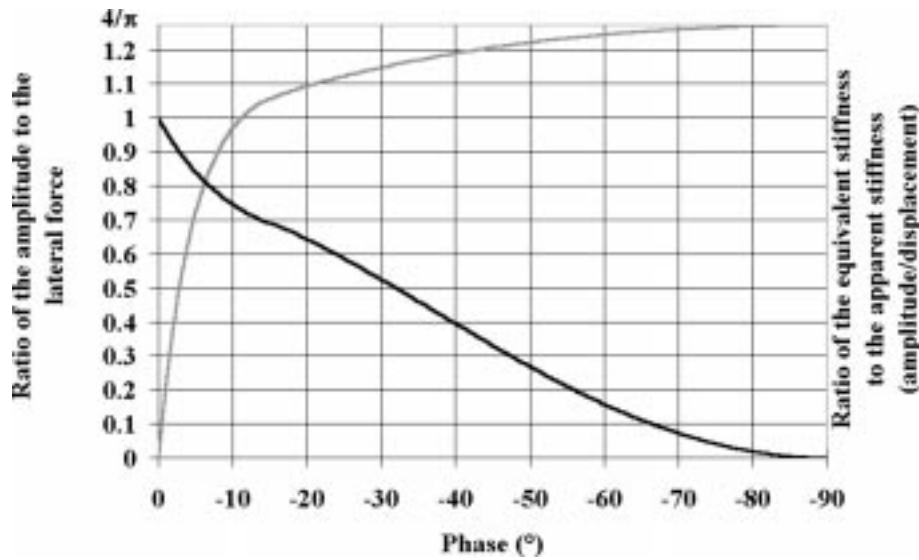


Figure 11. Ratio of the apparent stiffness (amplitude divided by the displacement) to the lateral system stiffness (black line) and of the ratio of the amplitude to the lateral force (gray line) as a function of the phase.

lock-in amplifier) and the friction force F_F , and, second, the apparent stiffness (defined as the ratio of the amplitude on the displacement d) and the lateral system stiffness. Figure 11 presents the ratio of the apparent system stiffness to the lateral system stiffness, and the ratio of the amplitude to the friction force, as a function of the phase. Then the phase signal allows us to correct the amplitude given by the lock-in amplifier. Using the value contained in figure 11, we are able to correct theoretically the amplitude image to give both a friction and an elastic image of the surface whatever the displacement may be.

6. Conclusions

Experimental and theoretical results of indirect FMM have shown that:

- (i) The classical “two Kelvin–Voigt” model is not efficient to explain experimental results because it does not take into account the lateral force.
- (ii) The influence of the lateral force, in a laser beam detection system, could lead to inverted contrast, compared to contrast predicted by the “two Kelvin–Voigt” model, and false interpretation of the image.
- (iii) Only high cantilever stiffness ($k_F > 10 \text{ N m}^{-1}$) should be used to obtain elastic contrast predicted by the “two Kelvin–Voigt” model.

A new model, which is able to explain experimental results, is proposed. This model shows that the response of the cantilever is a complex function of the contact stiffness, the lateral force and of the geometrical properties of the cantilever, and shows that Z -modulation imaging could not be easily used for true and quantitative elastic imaging.

To improve this problem, we propose to replace Z -modulation experiments by X -modulation experiments. This technique presents great advantages:

- (a) The LFM signal is used to realize imaging. This signal is only due to lateral force. Furthermore, this signal does not feed the servo loop. Consequently, no extra noise is added on images. There is no need of an extra piezo and it is possible to work at low frequencies.
- (b) The torsion stiffness of the cantilever is typically three orders of magnitude higher than the flexion stiffness. This property of cantilever allows us to work with low flexion cantilever stiffness and then low static normal applied force and low contact radius.
- (c) The amplitude and phase signal allows us to realize both friction and elastic imaging. The elastic and the friction image are easily quantified.
- (d) The normal force and then the contact stiffness is constant compared to Z -modulation. There is no problem of linearity.

Nevertheless this technique has two disadvantages:

- (1) We measure the shear modulus, that means that the Poisson ratio has a big influence on the determination of the elastic modulus.
- (2) The torsion stiffness should be known which is difficult for a triangularly shaped cantilever.

Acknowledgement

The authors are grateful to Frédéric Oulevey (Ecole Polytechnique Fédérale de Lausanne, Switzerland) for advises concerning piezos and helpful comments and discussion, and to Luc Carpentier (Ecole Centrale de Lyon, France) for providing samples.

Appendix A. Response of the cantilever for Z-modulation

A Z-modulation of the sample ΔS leads to a variation of the normal F_N and lateral F_L on the contact and then to the variation of a load ΔN and of the couple ΔM applied on the cantilever. The two forces are going to change the edge position ΔZ , the tilt $\Delta\Theta$ of the cantilever and the lateral movement ΔY of the tip (figure 8).

Applying shear, moment, slope and deflection for beams [22] we can write

$$\Delta\Theta = -\frac{\Delta NL^2}{2EI} + \frac{\Delta ML}{EI}, \quad (29)$$

$$\Delta Z = \frac{\Delta NL^3}{3EI} - \frac{\Delta ML^2}{2EI}, \quad (30)$$

with I the moment of inertia of the cantilever, E the Young modulus of the beam and L the length of the cantilever.

A.1. Low excitation

If we consider that the excitation is low enough, the response of the cantilever is sensitive to the lateral system stiffness:

$$\Delta N = k_N(\Delta S - \Delta Z), \quad (31)$$

$$\Delta M = Hk_L\Delta Y = -AH^2k_N\Delta\Theta, \quad (32)$$

with

$$A = \frac{k_L}{k_N}. \quad (33)$$

We put

$$n = \frac{k_N}{k_F}. \quad (34)$$

Furthermore the flexion stiffness for a rectangular beam is equal to

$$k_F = \frac{3EI}{L^3}. \quad (35)$$

By introducing equations (33)–(35) in equations (29) and (30) we find

$$\Delta\Theta = -\frac{3n}{2L}(\Delta S - \Delta Z) - 3An\left(\frac{H}{L}\right)^2 \Delta\Theta, \quad (36)$$

$$\Delta Z = n(\Delta S - \Delta Z) + \frac{3}{2}An\frac{H^2}{L}\Delta\Theta. \quad (37)$$

If we resolve this system of two equations, we find equation (25).

A.2. High excitation

If the excitation is high enough, M is no more proportional to the lateral system stiffness but to the friction force F_F :

$$\Delta N = k_N(\Delta S - \Delta Z), \quad (38)$$

$$\Delta M = HF_F, \quad (39)$$

then we can write

$$\Delta\Theta = -\frac{3n}{2L}(\Delta S - \Delta Z) + 3\frac{H}{L^2k_F}F_F, \quad (40)$$

$$\Delta Z = n(\Delta S - \Delta Z) - \frac{3}{2}\frac{H}{L^2k_F}F_F. \quad (41)$$

By resolving this system of two equations we find equation (26).

A.3. Limit between low and high excitation

In this chapter we are going to estimate the displacement ΔS which makes the limit between the partial slip (low excitation) and the total slip (high excitation). The total sliding is obtained for

$$\Delta Y > \frac{3F_F}{2k^*}, \quad (42)$$

with $\Delta Y = H\Delta\theta$. Furthermore, whatever n ,

$$\Delta\Theta < \frac{3\Delta S}{2L}, \quad (43)$$

so we can write

$$\frac{H}{L}\Delta S > \frac{F_F}{k^*}, \quad (44)$$

with

$$k^* = \left(\frac{1}{k_B} + \frac{1}{k_L}\right)^{-1}, \quad (45)$$

where k_B is the buckling cantilever stiffness. In every case $k^* < k_L$ then

$$\Delta S > \frac{F_F}{k_L} \frac{L}{H}. \quad (46)$$

Numerical applications show that the lateral movement of the tip is in total sliding for a typical value of ΔS equal to a few nanometers. We deduce that the contrast in Z-modulation image obtained with low cantilever stiffness is only sensitive to friction force.

Appendix B. Magnitude and phase as measured by a lock-in amplifier

To measure the magnitude M and the phase φ of a harmonic signal at the frequency ω , the lock-in amplifier releases a mathematical processing to extract the first harmonic component of the signal. This processing takes the signal $V(t)$ and multiplies it by two sine references:

$$A_2 = V(t)^* \cos(\omega t), \quad (47)$$

$$A_1 = V(t)^* \sin(\omega t). \quad (48)$$

The integration of these two signals between 0 and $2\pi/\omega$ gives X and Y which are the in-phase and out-phase coef-

ficients of the signal, respectively. The magnitude M and the phase φ of the signal are equal to

$$M = \sqrt{X^2 + Y^2}, \quad (49)$$

$$\varphi = \text{atan}(Y/X). \quad (50)$$

References

- [1] G. Binnig, C.F. Quate and C. Gerber, *Phys. Rev. Lett.* 56 (1986) 930.
- [2] C.M. Mate, G.M. McClelland, R. Erlandson and S. Chiang, *Phys. Rev. Lett.* 59 (1987) 1942.
- [3] S. Fujisawa, Y. Sugawara, S. Ito, S. Mishima, T. Okada and S. Morita, *Nanotech.* 4 (1993) 1.
- [4] R. Overney and E. Meyer, *MRS Bulletin* 18-5 (1993) 26.
- [5] J.L. Loubet, M. Belin, R. Durand and H. Pascal, *Thin Solid Films* 23 (1994) 194.
- [6] Y. Liu, T. Wu and D.F. Evans, *Langmuir* 10 (1994) 2244.
- [7] R.W. Carpick, N. Agrait, D.F. Ogletree and M. Salmeron, *Langmuir* 12 (1996) 3334.
- [8] J. Colchero, M. Luna and A.M. Baro, *Appl. Phys. Lett.* 68 (1996) 2896.
- [9] P. Maivald, H.J. Butt, S.A.C. Gould, C.B. Prater, B. Drake, J.A. Gurley, V.B. Elings and P.K. Hansma, *Nanotech.* 2 (1991) 103.
- [10] M. Radmacher, R.W. Tillmann and H.E. Gaub, *Biophys. J.* 64 (1993) 735.
- [11] R.M. Overney E. Meyer, J. Frommer, H.J. Güntherdot, M. Fujihira, H. Takano and Y. Gotoh, *Langmuir* 10 (1994) 1281.
- [12] N.A. Burnham, A.J. Kulik, P.J. Gallo, G. Gremaud and F. Oulevey, *J. Vac. Sci. Technol. B* 14 (1996) 794.
- [13] E.L. Florin, M. Radmacher, B. Fleck and H.E. Gaub, *Rev. Sci. Instrum.* 65 (1994) 639.
- [14] S.I. Yamamoto, H. Yamada, S.P. Jarvis, M. Motomatsu and H. Tokumoto, *Mater. Res. Soc. Symp. Proc.* 346 (1997) 385.
- [15] P.E. Mazeran and J.L. Loubet, *Tribol. Lett.* 3 (1997) 125.
- [16] M. Troyon, Z. Wang, D. Pastre, H.N. Lei and A. Hazotte, *Nanotech.* 8 (1997) 1.
- [17] N.A. Burham, G. Gremaud, A.J. Kulik, P.J. Gallo and F. Oulevey, *J. Vac. Sci. Technol. B* 14 (1996) 1308.
- [18] U. Rabe, K. Janser and W. Arnold, *Rev. Sci. Instrum.* 67 (1996) 3281.
- [19] K.L. Johnson, K. Kendall and A.D. Roberts, *Proc. Roy. Soc. London A* 324 (1971) 301.
- [20] B.V. Derjaguin, V.M. Muller and Y.P. Toporov, *J. Colloid Interface Sci.* 53 (1975) 314.
- [21] D. Maugis, *J. Colloid Interface Sci.* 150 (1992) 243; D. Maugis and B. Gauthier-Manuel, *J. Adhes. Sci. Technol.* 8 (1994) 1311.
- [22] R.J. Roark and W.C. Young, *Formulas for Stress and Strain* (McGraw-Hill, New York, 1975).
- [23] J.E. Sader, I. Larson, P. Mulvaney and L.R. White, *Rev. Sci. Instrum.* 66 (1995) 3789; K.E. Petersen, *Proc. of the IEEE* 70 (1982) 420; D.F. Ogletree, R.W. Carpick and M. Salmeron, *Rev. Sci. Instrum.* 67 (1996) 3298.
- [24] R. Lakes, *Science* 235 (1987) 1038; D. Prall and R. Lakes, *Int. J. Mechanical Sci.* 39 (1996) 305.
- [25] T. Göddenhenrich, S. Müller and C. Heiden, *Rev. Sci. Instrum.* 65 (1994) 2870.
- [26] K. Yamanaka and E. Tomita, *Jpn. J. Appl. Phys.* 34 (1995) 2882.
- [27] R.M. Overney, H. Takano and M. Fujihira, *Europhys. Lett.* 26 (1994) 443.
- [28] R.W. Carpick, D.F. Ogletree and M. Salmeron, *Appl. Phys. Lett.* 70 (1997) 1548.
- [29] C. Frétygny, C. Basire and V. Granier, *J. Appl. Phys.* 82 (1997) 43.
- [30] K.J. Wahl, S.V. Stepanowski and W.N. Unertl, *Tribol. Lett.* 5 (1998) 103.
- [31] C. Basire and C. Frétygny, *Eur. Phys. J. AP* 6 (1999) 323.
- [32] D.F. Ogletree, R.W. Carpick and M. Salmeron, *Rev. Sci. Instrum.* 67 (1996) 3298.
- [33] A. Noy, C.D. Frisbie, L.F. Rozsnyai, M.S. Wrighton and C.M. Lieber, *J. Am. Chem. Soc.* 117 (1995) 7943.
- [34] J.P. Cleveland, S. Manne, D. Bocek and P.K. Hansma, *Rev. Sci. Instrum.* 64 (1993) 403.
- [35] D.J. Keller and F.S. Franke, *Surf. Sci.* 294 (1993) 409.
- [36] J.S. Villarubia, *Surf. Sci.* 321 (1994) 287.
- [37] N. Bonnet, S. Dongmo, P. Vautrot and M. Troyon, *Microsc. Microanal. Microstruct.* 5 (1994) 477.
- [38] L. Odoni, M. Boehm, P.E. Mazeran and J.L. Loubet, to be submitted.
- [39] R.D. Mindlin, *Trans. ASME, Serie E, J. of Applied Mechanics* 16 (1949) 259.
- [40] A.R. Savkoor, *Dry Adhesive Contact of Elastomers* (Technische Universiteit Delft, Delft, 1987).
- [41] K.L. Johnson, *Proc. Roy. Soc. London A* 453 (1997) 163.
- [42] R.D. Mindlin, W.P. Mason, J.F. Osmer and H. Deresiewicz, in: *Proc. 1st US National Congress of Applied Mechanics*, New York, USA (1954) p. 203.